


# Technical Evaluation of a Superconducting Fault Current Limiter for a Microgrid with Wind-PV Hybrid Generation

Saad A. Mohamed Abdelwahab\*<sup>‡</sup> , Sherif S. M. Ghoneim\*\* , A. M. Hamada \*\*\* , Saady Hasan\*\*\*\* , Ragab Khamis\* , Walid S. E. Abdellatif \* 

\* Electrical Department, Faculty of Technology and Education, Suez University, Suez 43527, Egypt

\*\*Department of Electrical Engineering, College of Engineering, Taif University, P. O. Box 11099, Taif 21944, Saudi Arabia;

\*\*\* Electrical Department, Faculty of Technological, Higher of Ministry, Alex., Egypt.

\*\*\*\*Department of Electrical Engineering Faculty of Engineering, Helwan University

(saad.abdelwahab@suezuniv.edu.eg, s.ghoneim@tu.edu.sa, abdallahmhe@yahoo.com, ahsaady500@gmail.com, dr.ragabsalem@gmail.com, Walid.Abdellatif@suezuniv.edu.eg)

<sup>‡</sup> Corresponding Author; Saad A. Mohamed Abdelwahab, 43527, Tel: +201096250375,  
[Saad.Abdelwahab@suezuniv.edu.eg](mailto:Saad.Abdelwahab@suezuniv.edu.eg)

*Received: 28.09.2023 Accepted:02.11.2023*

**Abstract-** The integration of fault current limiters (FCLs) with microgrids has received significant because of their capacity to improve the reliability and stability of microgrid systems. The main focus of the research is to improve the protection of the microgrid by reducing the fault current and minimizing the impact of fault events. This study presents an investigation into the performance enhancement of superconducting fault current limiter (SFCL) within a microgrid context. The research delves into the effects of various fault types, making angles, and fault locations on the SFCL's functionality. The study will reveal SFCL's consistent and effective current limiting capabilities across these diverse fault scenarios. Understanding this effect crucial for optimizing SFCL performance. Regarding the effect of fault locations, the study investigated fault occurrences near loads, the grid, and renewable energy sources within a Microgrid system. The results consistently showcased SFCL's ability to limit fault currents irrespective of fault locations, ensuring system stability and reliability. The collective insights gained from this study contribute significantly to the understanding of SFCL's role in enhancing power system performance and resilience. The significance of utilizing hybrid sources of wind, solar, and conventional energy, and their impact on specific fault current performance, or whether a fault current limiter has been successfully able to handle them, along with provided values or percentages demonstrating its proven effectiveness, holds utmost importance. The findings provide valuable guidance for power system engineers, aiding in the strategic allocation and deployment of SFCLs for improved power network management. This paper advances the knowledge surrounding SFCLs' applicability and effectiveness within Microgrid environments, paving the way for more secure and efficient energy systems.

**Keywords-** FCL; SFCL; Microgrid; Wind farm and Wind-PV Hybrid Generation

## 1. Introduction

Microgrids are emerging as a promising solution for reliable and efficient power delivery in modern power systems. A small-scale power system known as a microgrid can independently or be connected to the main grid [1-2]. The combination of renewable energy sources and distributed generators in microgrids has significantly increased their complexity and introduced new challenges related to power quality and protection. FCLs have been proposed as an effective solution for enhancing the protection and stability of microgrids by limiting the fault current during fault events. FCLs are devices that can temporarily increase their impedance during fault events to limit the current flow and reduce the system's effects of the failure. The integration of

FCLs with microgrids has attracted a lot of attention recently, and various studies have been conducted to investigate the performance enhancement and optimal allocation of FCLs in microgrids [3-5].

The expansion of power systems has led to a rise in the adoption of SFCLs for mitigating fault currents [6]. The Power systems are designed with low impedances between generations and loads, resulting in substantial fault currents, often ranging from 5 to 20 times the nominal current during fault conditions. In fault scenarios, SFCLs serve essential purpose is restraining fault currents and swiftly restoring them to normal levels once the fault is cleared. This restoration to standard operating conditions post-fault removal has also been observed [7].

Implementing FCLs comes with various challenges. These include integrating them with existing grid infrastructure, ensuring proper coordination with other protective devices, achieving fast responses without compromising stability, managing voltage drops during operation, handling high fault currents, accurate fault detection, addressing temperature effects, managing costs and maintenance, integrating with renewable sources, establishing standards and regulations, and accurate modeling to validate the simulation results. Addressing these challenges is crucial for the effective deployment of FCLs in power systems [8]. Among these solutions, SFCLs have gained significant attention for their potential to enhance power system stability and reliability. SFCLs act as protective devices that limit fault currents, mitigating the adverse effects of short-circuit faults and ensuring uninterrupted power supply [9].

In recent years, Microgrid have emerged as a promising paradigm for modern power distribution. These localized energy networks integrate various distributed energy resources, including renewable sources such as wind and photovoltaic (PV) systems. [4].

The enhancement of transient performance in a microgrid through the application of a resistive SFCL [1]. The investigate how this limiter positively influences the transient behavior of the microgrid. Its focuses on the benefits of integrating such a limiter in terms of improved system stability and performance during transient events. The understanding of how resistive SFCL can effectively enhance the dynamic response of microgrids, potentially leading to more reliable and resilient power distribution systems [1].

The conducts a feasibility analysis regarding the optimal placement of SFCLs within a smart grid context [2]. Through the use of simulation tools like simulink they investigate the potential positioning of SFCLs to enhance the performance of the smart grid. It delves into the practicality and effectiveness of integrating SFCLs into smart grid systems, providing insights into how these devices can contribute to the overall stability, reliability, and efficiency of modern power distribution networks [2].

The comparative analysis of two significant technologies SFCLs and dynamic voltage restorers, with a focus. On enhancing the high-penetration microgrids' low voltage ride through capability. It involves assessing the effectiveness of SFCLs and DVRs in mitigating voltage and current disruptions triggered by faults within microgrid systems [3].

Previously, shunt reactors were employed to curb current levels. However, in certain cases, these devices had to curtail fault currents, thus presenting a limitation [8]. These reactors possessed fixed impedance, leading to constant load implications [9]. In power systems, SFCL finds utility, particularly in transmission and distribution networks, to mitigate the impacts of grid turbulences. In the context of smart grids, SFCLs emerge as pivotal devices for ensuring grid protection [9].

In [11], to enhance the protection and reliability of power systems by strategically placing SFCLs to optimize fault current limitation. Through examination of the effects of SFCL placement on the electric power system's outcomes, the study offers suggestions for enhancing efficiency of fault current management in systems with distributed generations.

The focuses on studying how SFCLs can be effectively integrated into power systems to enhance their performance and reliability [12]. By conducting application studies, the explore the potential benefits, challenges, and outcomes of employing SFCLs in real-world power systems [12].

In [13], the presents an experimental investigation into the performance of. An SFCL in a system with double circuit transmission lines. Its focuses on evaluating the SFCL's ability to effectively limit fault currents in a complex transmission line scenario. By conducting experiments, the s explores the behavior of the SFCL under different fault conditions and operating scenarios. the offers insightful information on the practical implementation and effectiveness of SFCLs in enhancing the reliability and stability of double circuit transmission line systems [13].

The focuses on optimizing the interaction between SFCLs and protection mechanisms to strengthen the performance and system dependability for power transmission [14]. By analyzing the coordination strategies and their impact on fault current limitation and protection, the contribute to the understanding of effective methods for integrating SFCLs into transmission line systems. The provides insights into the practical implementation of SFCLs in coordination with existing protection schemes to improve the overall security and stability of power transmission networks [14].

The assessment of the high-temperature SFCL capability to restore its superconducting state and operational efficiency subsequent to encountering fault events [15]. By scrutinizing the recovery response when subjected to varying loads, the authors offer valuable perspectives into the dependability and efficiency of employing second-generation FCL within power transmission contexts. Its significantly enriches the comprehension of the dynamic conduct and recuperative potential of HTS fault current limiters, pivotal elements that safeguard the stability and operational effectiveness of power transmission systems [15].

This paper is dedicated to analysis the performance enhancement of SFCLs within the context of Microgrid. The primary goals of this research are to investigate impacts of various fault types, making angles, and fault locations on SFCLs' functionality. By doing so, this research contributes to a comprehensive understanding of how SFCLs can be effectively utilized to safeguard Microgrid systems. The paper is also interested in designing an SFCL this may lower the fault current and improve the stability of the microgrid during fault events.

The subsequent sections of this paper delve into the detailed analysis of these effects. Section 2 system description, microgrid. Section 3, analysis and design of proposed FCL, provides an overview of the fundamental concepts of SFCLs presents the methodology used for simulation and analysis. Sections 4, the effects of fault types, making angles, and fault locations on SFCL performance. Finally, conclusions

## 2. Description of the Proposed System

The system under investigation in this paper comprises a Microgrid integrated with SFCLs, aimed at enhancing system stability and fault management. The Microgrid is a localized energy network that incorporates various distributed energy resources, including renewable sources such as wind and PV

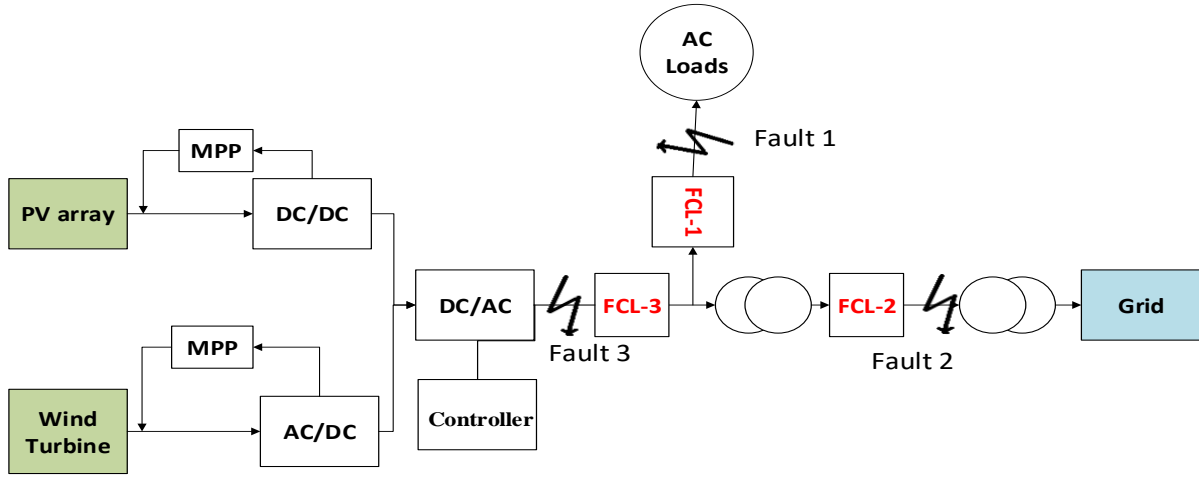


**Fig.1.** The proposed system of Microgrid with SFCL.

systems. These resources contribute to the generation of electrical power within the Microgrid. To analyze the impact of fault types, making angles, and fault locations on the performance of SFCLs, the researchers employ simulation tools and technical evaluation. These simulations involve inducing faults of varying type's symmetrical and unsymmetrical fault at different locations within the Microgrid. The making angles, representing the point in the waveform at which a fault occurs, are also manipulated to understand their influence on SFCL operation.

Through comprehensive simulation studies, this paper aims to elucidate the behavior of SFCLs under different fault scenarios. The fault making angle indicates the angle at which the fault occurs starting from zero source voltage. It's well-known that this angle has a pronounced impact on the rate of growth of current (di/dt) and the peak fault current value. The short-circuit current reaches the highest value it can have,  $I_{max}$ . When zero voltage is crossed, if the circuit is closed. The results obtained from these simulations provide valuable insights into the optimal allocation and utilization of SFCLs within Microgrid. Such insights contribute to the advancement of power distribution systems, particularly in terms of fault management and system stability.

**2.1 Wind turbine**

The wind energy system comprises wind turbines with variable speeds with a partial-rating power transformer and incorporates a promising technology known as the doubly fed induction generator (DFIG). The configuration of the suggested system is compatible with changing wind turbines and includes a partial-scale frequency converter connected to the network. The power output of wind turbines is determined by the wind speed [16- 18]. Kinetic energy (E), which is the result of equation (1), is used to create wind energy. In order to separate the kinetic energy in the wind, as described in equation (2), wind energy can be acquired. The wind mass flow rate needed to generate electricity is determined by equation (3). Wind energy can be written as equation (4) by swapping equations (3) for equations (2).

$$E = \frac{1}{2} \dot{m} * V^2 \tag{1}$$

$$P = \frac{dE}{dt} = \frac{1}{2} \dot{m} * V^2 \tag{2}$$

$$\dot{m} = \rho Av \tag{3}$$

$$p = 0.5 \rho Av^3 \tag{4}$$

Equation (5) can be used to determine the real mechanical capacity to produce wind energy received from wind turbines. While the mechanical torque can be determined using equation (6).

$$P_m = C_p(\lambda, \beta) \frac{A \rho v^3 w}{2} \tag{5}$$

$$T_m = \frac{P_m}{w_m} \tag{6}$$

Where,  $C_p$ : The power coefficient, is mechanical power, P : The mechanical power,  $\dot{m}$ : The air mass,  $\rho$ : The density of air, V: The wind speed (m/s), A: The swept area, R: The wind turbine rotor radius,  $C_p$ : The related to and tip speed ratio ( $\lambda r$ ) and  $T_m$ : The mechanical torque (Nm).

The doubly fed induction generator (DFIG) model is fully defined in [19]. The following equation describes the voltage equations in the d-q reference

$$V_{ds} = R_s i_{ds} - \omega_s \lambda_{qs} + \frac{d\lambda_{ds}}{dt} \tag{7}$$

$$V_{qs} = R_s i_{qs} - \omega_s \lambda_{ds} + \frac{d\lambda_{qs}}{dt} \tag{8}$$

$$V_{dr} = R_r i_{dr} - (\omega_s - \omega_r) \lambda_{qr} + \frac{d\lambda_{dr}}{dt} \tag{9}$$

$$V_{qr} = R_r i_{qr} + (\omega_s - \omega_r) \lambda_{dr} + \frac{d\lambda_{qr}}{dt} \tag{10}$$

The Stator and rotor flux as follow:

$$\Phi_{ds} = L_s i_{ds} + M i_{dr} \tag{11}$$

$$\Phi_{qs} = L_s i_{qs} + M i_{qr} \tag{12}$$

$$\Phi_{dr} = L_r i_{dr} + M i_{ds} \tag{13}$$

$$\Phi_{qr} = L_r i_{qr} + M i_{qs} \tag{14}$$

The electromagnetic torque, stator, rotor, active and reactive power as follows:

$$T_{em} = \frac{3}{2} p (\Phi_{ds} i_{qr} - \Phi_{qs} i_{dr}) \tag{15}$$

$$P_s = \frac{3}{2} (v_{ds} i_{ds} + v_{qs} i_{qs}) \tag{16}$$

$$Q_s = \frac{3}{2} (v_{qs} i_{ds} - v_{ds} i_{qs}) \tag{17}$$

$$P_r = \frac{3}{2} (v_{dr} i_{dr} + v_{qr} i_{qr}) \tag{18}$$

$$Q_r = \frac{3}{2} (v_{qr} i_{dr} - v_{dr} i_{qr}) \tag{19}$$

where;  $V_{ds}, V_{qs}, V_{dr}, V_{qr}, I_{ds}, I_{qs}, I_{dr}, I_{qr}, \lambda_{ds}, \lambda_{qs}, \lambda_{dr}, \lambda_{qr}, \Phi_{ds}, \Phi_{qs}, \Phi_{dr}, \Phi_{qr}, P_s, Q_s, P_r, Q_r,$  and  $L_r, M$  represents the stator and rotor voltages, currents, fluxes active and reactive power, mutual inductances in the d-q axis respectively.

2.2 PV model

Today, there is a global trend towards using clean energy to replace fossil fuels with renewable sources that emit no pollutants. When designing and analyzing photovoltaic control systems, mathematical models for PV panels play a crucial role. The current-voltage characteristic of a PV cell can be described by an equation [20-21]:

$$I_c = I_{ph} - I_o \left\{ e^{\left[ \frac{q}{AKT}(V_c + I_c R_s) \right]} - 1 \right\} \tag{20}$$

$$V_c = \frac{AKT}{q} \ln \left( \frac{I_{ph} + I_o - I_c}{I_o} \right) - I_c R_s \tag{21}$$

$$I = I_{ph} - I_o \left\{ e^{\left[ \frac{q}{n_s AKT}(V + n_s I R_s) \right]} - 1 \right\} \tag{22}$$

$$V = \frac{n_s AKT}{q} \ln \left( \frac{I_{ph} + I_o - I}{I_o} \right) - n_s I R_s \tag{23}$$

Where;

$$I_{ph} = \frac{G}{1000} [I_{sc} + k_i (T - T_r)] \tag{24}$$

$$I_o = I_{or} \left( \frac{T}{T_r} \right)^3 e^{\left[ \frac{qE_g}{AK} \left( \frac{1}{T_r} - \frac{1}{T} \right) \right]} \tag{25}$$

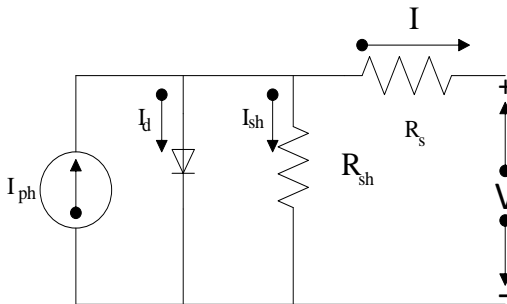


Fig.2. PV cell equivalent circuit [21].

where,  $V_c$  is cell PV voltage (V),  $I_o$  is diode current (A),  $I_{or}$  is diode saturation current (A),  $V$  is diode voltage (V),  $K$  is constant of boltzmann =  $1.3806 \cdot 10^{-23}$  J.K-1,  $n_1$  is diode factor of ideality up to 1.0,  $q$  is charge of electron =  $1.6022 \cdot 10^{-19}$ ,  $G$  is solar radiation and  $T$  is cell temperature (C°).

2.3 DC-DC boost converter

As was already said, the PV generation resource's output voltage is determined. To accommodate the relatively low voltage and power levels generated by the PV panel, a DC/DC boost converter. Is used to increase the voltage to the proper amount. The three-phase inverter that is linked to the grid or an AC load transforms this increased DC voltage into AC. [22].

2.4 Controller on three-phase inverter

The controller system depicted in Fig. 3 comprises four simultaneous control loops. The first step is to apply Park's transformation to convert the stationary reference frame

voltages and currents into the matching spinning reference frame values. The second control loop then compares the currents to the specified references. With the reference current set to zero to maximize the amount of power delivered to the grid and keep the voltage source inverter (VSI) working at a unity power factor, the third loop is in charge of controlling the AC voltage to manage the magnitude of the AC voltage from the VSI. In this third loop, the regulator is supplied the measured DC-link capacitor voltage to establish the d-axis current instruction. The fourth loop involves the PWM block, which receives signals from the current regulators and transmits them to the VSI electronic switches. [17-21].

The integration of a SFCL into the system can enhance its performance. In this context, the SFCL can be incorporated into the controller system described in Fig. 3 to improve grid stability and mitigate fault currents.

The SFCL can be positioned strategically within the system to detect and respond to fault conditions. The SFCL can quickly restrict the fault current when a problem arises, protecting the system components and preventing excessive stress on the voltage source inverter (VSI) and associated equipment. This integration with SFCL enhances the overall system's fault tolerance and transient performance, ensuring that the grid operates smoothly even during fault events. The controller system described earlier can work in coordination with the SFCL, sharing information about fault conditions and adjusting control parameters as needed to optimize the system's response to faults and maintain stability. The precise details of this integration would depend on the specific characteristics and requirements of the SFCL and the overall system design.

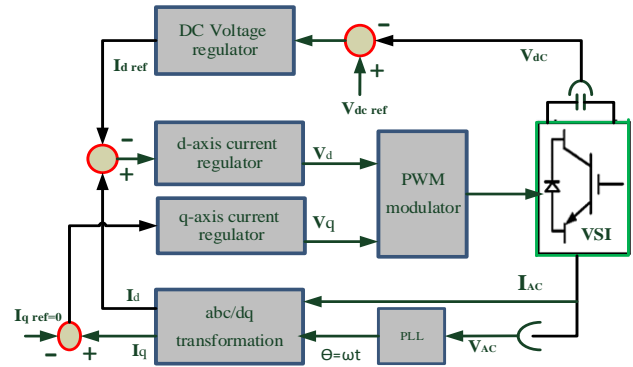


Fig. 3. Block schematic for a system's inverter controller.

3. Analysis and Design of Proposed FCL

The circuit consists of three parallel paths as showing in Fig. 4:

- The first path is the main path that contains the main switch, through which the current flows in normal conditions.
- The second path is the alternative path in case of a fault, and it consists of two thyristors, T1 and T2.
- The third path is the damping circuit, which consists of diodes D1 and D2, two thyristors T3 and T4, a coil, and a capacitor.

The basic idea of how the circuit works relies on the current value flowing through it.

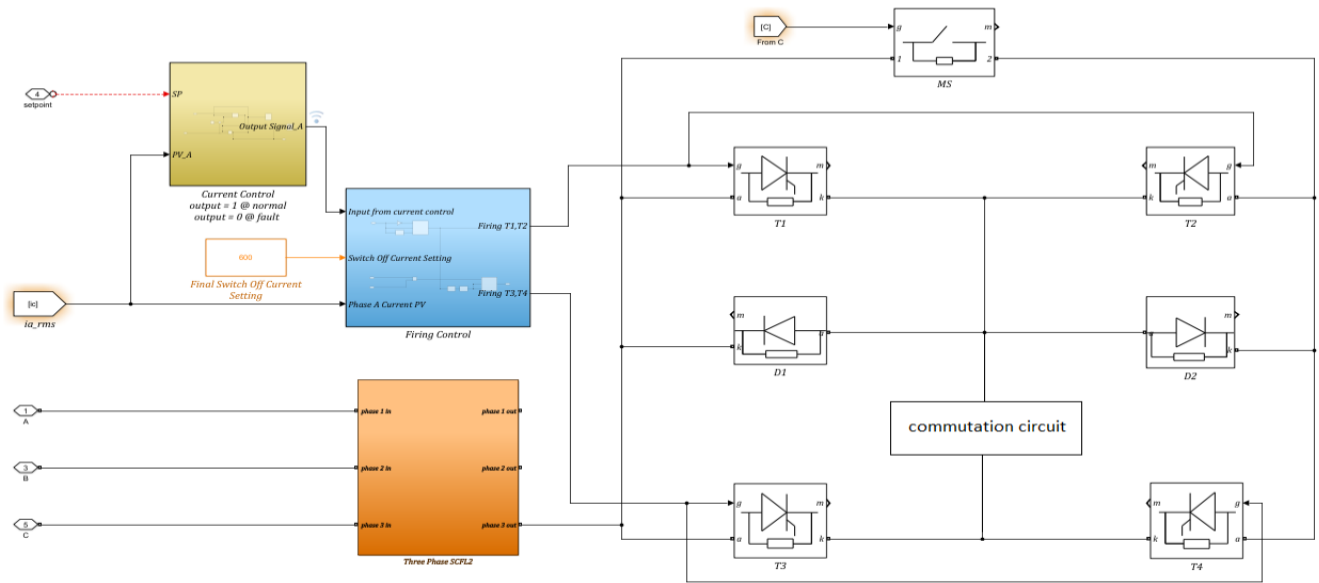


**Fig. 4.** Proposed circuit of SFCL.

In normal conditions, the mechanical switch on the first path has current flowing through it. The control circuit operates by comparing the normal current with setpoint value known as the "setpoint."

Whenever there is a problem, the control circuit sends a signal to either T1 or T2 depending on the fault's polarity (positive or negative), and the alternative path is opened.

Immediately after that, another control signal is sent to activate either T3 or T4, allowing the current to pass through the damping circuit. Simultaneously, the contact points of the mechanical switch in the first path are opened.

### 3.1 Operating Principle of FCL

The research introduces hybrid concept of FCL that employs a stand-alone switching module to transmit gateway signals through a controller [23].

The electrical power SFCL operates using a technique known as forced current commutation. In order to swiftly stop fault currents, this method requires injecting a counter-current into the circuit breaker's primary contacts. High-power semiconductors and quick mechanical contact movements are both used in it. To validate the operational characteristics of this approach, the operational principle and complete opening sequence of the three-phase SFCL, along with the control signal of IGBTs (Integrated Gate-Commutated Thyristors), are illustrated.

The principle of forced commutation is employed to interrupt the current in a manner that avoids the challenges posed by rapidly bringing high short-circuit currents to zero.

This can be challenging because arc plasma exists between the major contacts. The forced commutation principle moves the current from the fast-opening switch to a shunt commutation circuit rather than suddenly stopping the fault current flow. Within the shunt commutation circuit, which includes commutation inductance and capacitance components, the current undergoes, a slow decrease after a brief time to zero. This approach allows for a more controlled

and manageable interruption of the fault current while minimizing the impact of arc plasma between the main contacts.

Figure 5 show the flowchart of the proposed model with SFCL. The interruption tests delve into how well the SFCL manages to interrupt fault currents once they are detected. This is a critical aspect of the SFCL's function, as successful interruption prevents damage to system components and aids in quick fault recovery. The interruption tests analyze factors such as the type of fault, the timing of fault occurrence, and the SFCL's response time. The results obtained from these tests provide valuable insights into the SFCL's practical applicability in real-world scenarios. They validate the SFCL's performance in limiting and interrupting fault currents effectively, enhancing the overall reliability and stability of the Microgrid. Additionally, these tests offer a deeper understanding of how the SFCL interacts with different fault conditions and aids in refining the model for optimal performance. The combination of current commutation and interruption tests serves as a pivotal step in bridging the theoretical concepts of the proposed SFCL model with its practical implementation. These tests provide empirical evidence of the SFCL's capabilities and contribute to the validation of its effectiveness as a fault management solution within the Microgrid context.

### 3.2 Theoretical Analysis and Design of SFCL

The cornerstone of SFCL operation is the critical current, denoted as  $I_c$ . The superconducting state is lost and the material reverts to a resistive state when a superconductor's critical current value is exceeded. This transition is known as a quench. Two primary mechanisms come into play: thermal and magnetic quenching. When a superconductor's temperature increases as a result of an excessive current flow, thermal quenching takes place. While magnetic quenching is triggered by an external magnetic field surpassing a critical threshold. It's essential to consider three critical factors:



temperature, electrical field, and current because exceeding any of these values can result in a loss of superconductivity, as depicted in Fig. 6. The operation modes of the SFCL can be categorized into three modes based on resistance values, along with a fourth mode, which signifies the recovery to the superconducting state, as illustrated in Fig. 7.

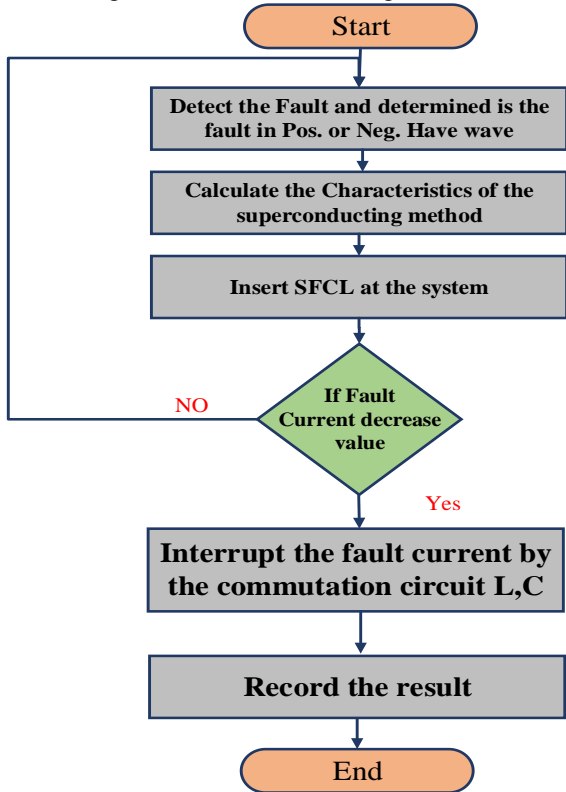


Fig. 5. Flowchart of the proposed model with SFCL

In the superconducting state, the material exhibits zero resistance at current density "I" and temperature "T" below their critical values, denoted as "I<sub>c</sub>" and "T<sub>c</sub>." When the current density surpasses "I<sub>c</sub>," the superconductor transitions into a flux flow state, leading to significant heating. Once the superconductor's temperature exceeds "T<sub>c</sub>," it switches to a normal conducting state, and its resistance increases with rising temperature. The quenching process in the superconducting material results in the generation of residual heat, even after the current is reduced below the critical value. This heat needs to be removed by the cryogenic cooling system. Typically, there's a temporary temperature rise in the superconducting material, causing a loss of superconductivity until the cryogenic system can restore the material's operating temperature. This time interval is known as the recovery period and is a significant differentiating parameter among various SFCL designs, as discussed in reference [24-31].

When a fault current occurs, the device rapidly transitions from a superconducting to a resistive state, thus limiting the current. Key components of an SFCL include superconducting elements, a cryogenic cooling system, and a trigger mechanism.

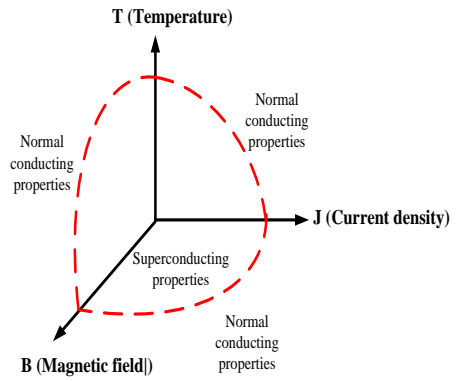


Fig.6. T-B-J Characteristics of SC material [3].

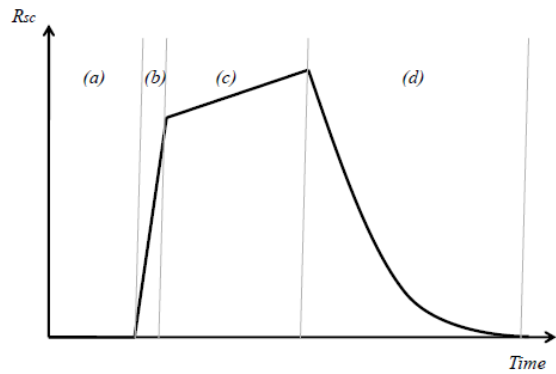


Fig.7. Modes of the SFCL Resistance of the superconducting element

The critical current, I<sub>c</sub>, can be calculated using the Ginzburg-Landau theory:

$$I_c = \Phi_0 / (2\pi\xi L) \tag{26}$$

where:

Φ<sub>0</sub> is the magnetic flux quantum.

ξ is the coherence length of the superconductor.

L is the length of the superconductor.

The inductance of an SFCL coil can be calculated using:

$$L = \mu_0 N^2 A / \ell \tag{27}$$

Equations for fault current estimation for each type of SFCL, specific equations can be used to estimate fault current limiting performance. These equations consider parameters such as system voltage (V<sub>s</sub>), system impedance (Z<sub>s</sub>), SFCL resistance or impedance (R<sub>SFCL</sub>, Z<sub>SFCL</sub>), and thyristor impedance (Z<sub>T</sub>) in the case of TC-SFCLs.

$$R - SFCL: I_f = (V_s - R_{SFCL} * I_f) / Z_s \tag{28}$$

$$SIC-SFCL: I_f = (V_s - Z_s * I_f) / (Z_s + Z_{SFCL}) \tag{29}$$

$$TC-SFCL: I_f = (V_s - Z_s * I_f) / (Z_s + Z_{SFCL} + Z_T) \tag{30}$$

The critical parameter for superconducting fault current limiters is their critical current (I<sub>c</sub>). It can be defined by the BCS theory, which relates critical temperature (T<sub>c</sub>) and the energy gap (Δ) as follows:

$$I_c = (\pi * \Delta) / (2 * e * R) \tag{31}$$

Where,  $I_c$  is the critical current,  $\pi$  is the mathematical constant Pi,  $\Delta$  is the energy gap,  $e$  is the elementary charge and  $R$  is the resistance of the superconductor, To calculate the voltage across a superconducting fault current limiter during a fault, you can use Ohm's law:

$$V = I * R \tag{32}$$

where,  $V$  is the voltage across the SFCL,  $I$  is the current flowing through the SFCL and  $R$  is the resistance of the SFCL in the quenched state. The following equation can be used to describe the critical current density ( $J_c$ ):

$$J_c = J_{c0} * [1 - (T/T_c)^2] \tag{33}$$

Where,  $T_c$  is the critical temperature of the superconductor, and  $J_{c0}$  is the greatest critical current density at absolute zero temperature ( $T=0K$ ).

Using equation (1), the superconductor's temperature is calculated. where the term  $E(t, T)$  (contained within  $Q_{sc}(t)$ ) is computed based on the methods described in references [25, 26], in the area of flux flow (where  $E(t, T) \geq E_0$  and  $T(t) < T_c$ ). When  $T(t) \geq T_c$ , it is expected that the superconductor quenches. Equation (34) is spelt out as,

$$T(t) = T_a + \frac{1}{C_{sc}} \int_0^t [Q_{sc}(t) - Q_{removed}(t)] dt \tag{34}$$

$$\frac{dT}{dt} = \frac{1}{C_{sc}} [Q_{sc}(T) - Q_{removed}(t)] \tag{35}$$

$$\frac{dT}{dt} = \frac{1}{C_{sc}} [i(t) E(t,T) I_{sc} - \frac{T(t)-T_a}{\theta_{sc}}] \tag{36}$$

As a result,  $E$  can be stated more simply as a function of temperature as follows:

$$\int dt = \int \frac{dT}{C_{sc} [i(t) E(t,T) I_{sc} - \frac{T(t)-T_a}{\theta_{sc}}]} \tag{37}$$

where,  $E(T)$  is formulated as [17],

$$E(T) = E_0 \left(\frac{E_c}{E_0}\right)^{\frac{\beta}{n}} \left(\frac{J_{c77K}}{J_c(T)}\right) \left(\frac{J(t)}{J_{c77K}}\right)^{\beta} \tag{38}$$

substituting (30) into (38) gives

$$E(T) = E_0 \left(\frac{E_c}{E_0}\right)^{\frac{\beta}{n}} \left(\frac{T_c-77}{T_c-T}\right) \left(\frac{J(t)}{J_{c77K} a_{sc}}\right)^{\beta} \tag{39}$$

In addition to  $I$  and  $ISC$  from equation (40), the non-temperature-dependent portion of  $E(T)$  can be combined as follows for convenience, as stated in reference [4]:

$$IE(T) I_{sc} = k \frac{T_c-77}{T_c-T} \tag{40}$$

$$k = IE_0 \left(\frac{E_c}{E_0}\right)^{\frac{\beta}{n}} \left(\frac{J(t)}{J_{c77K} a_{sc}}\right)^{\beta} I_{sc} \tag{41}$$

This expression yields a formula for "t," which represents the time it takes for the superconducting fault current to reach a specific temperature, denoted as "T."

Equation (39) can be solved using the method described in (41), as detailed in the subsequent subsection, with the constant "C" provided in equation (42).

$$t = C_{sc} \int \frac{dT}{\left[ k \frac{T_c-77}{T_c-T} - \frac{T-T_a}{\theta_{sc}} \right]} \tag{42}$$

The equation can be simplified to the form indicated in equation (43) in the typical scenario when liquid nitrogen is used as the cryogen.

$$t = C_{sc} \theta_{sc} \frac{\arctan\left(\frac{3}{\sqrt{20_{sc} k-9}}\right)}{\sqrt{20_{sc} k-9}} \tag{43}$$

#### 4. Simulation Results and Discussions

##### 4.1 Effect of fault types on the performance SFCL

The type of fault is one of the factors that significantly impact small electrical networks. As a result, it is essential to analyze this kind of risk in order to ascertain how much current will flow when a failure occurs. To ensure that loads and networks can sustain this problem, it is necessary to determine the maximum value of the short-circuit current. To provide adequate protection, it is also vital to identify the right kind of circuit breaker for this current. In this paper, an examination of many faults such as symmetrical and unsymmetrical, in order to analyze and understand their characteristics more deeply.

##### 4.1.1 Single Line to Ground Fault

Figure 8 illustrates the simulation results for a single line-to-ground (SLG), (Line A to Ground) when SFCL is activated. It is evident from this figure that the current  $I_A$  exceeds the  $I_{max}$  value or the pre-defined current discrimination value. In such a case, the control circuit sends a signal to the thyristor, causing it to open an alternative path to the original path (mechanical switch). The switching circuit is also activated, causing the capacitor to discharge its charge during the mechanical switch opening, reducing the voltage across the switch terminals and preventing any arcing during the opening.

Figure 8 illustrates the current on Phase A during a one-sided fault application between Phase A and ground. It is observing an increase in the current at time 0.307, surpassing the set value for SFCL activation, which is 4000 amperes. Subsequently, the current value is reduced by applying a reverse voltage of 1300 volts across the mechanical switch terminals, until it reaches a level that can be safely interrupted without any arcing. This process took place from the moment the fault started until it was cleared at time seconds.

The protective device's ability to limit the excess current is evident, and afterward, the mechanical switch can be safely opened without causing any arcing. When using the SFCL, the results clearly display the current and voltage waveforms.

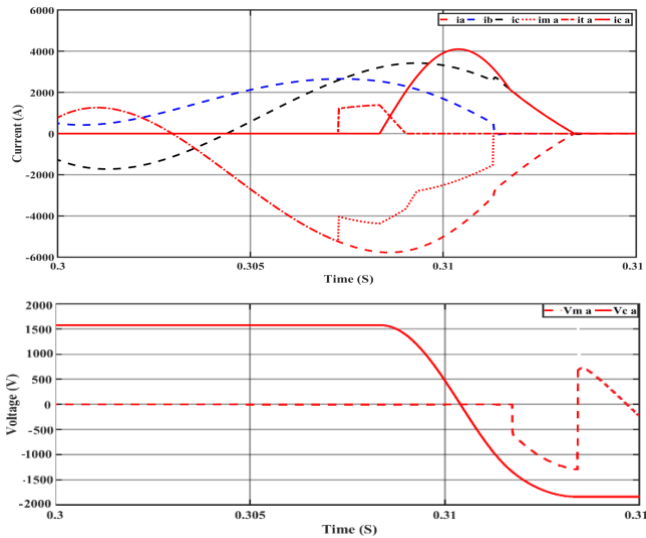


**Fig.8.**Current and voltage waveforms using SFCL at SLG fault at phase A

**4.1.2 Line to Line Fault (L-L Fault)**

The results of the simulation show the waveforms of current and voltage during the SFCL's implementation. The simulation results for a double line fault scenario (Line A to Line B) are shown in Figure 9. When SFCL is activated, it becomes evident from these figures that the current in both phases  $I_A$  and  $I_B$  goes above the  $I_{max}$  value or the pre-defined current discrimination value. In the case of a double line fault, SFCL completely interrupts the fault current in both phases. Figure 9 illustrates the current on Phases A and B during a fault application on both phases. We observe a significant increase in current at time 0.345, where the current reached a value of  $1.1 \times 10^4$  amperes. A reverse voltage of 1300 volts was applied across the mechanical switch terminals to reduce the current to a level that could be safely interrupted without any arcing. This process took place from the moment the fault started until it was cleared at time 0.09 seconds.

Figure 9, show simulation results for three different double line fault scenarios: Line A to Line B, Line A to Line C, and Line B to Line C. In all these scenarios, when SFCL is applied, the current in all phases  $I_A$  and  $I_B$  surpasses the  $I_{max}$  or the predefined selectivity current value. This indicates that for a double line fault, SFCL effectively interrupts the fault current in both affected phases, ensuring protection against this type of fault.

**4.1.3 Three Phase Faults**

Symmetrical faults occur in the system when there are faults in all three phases. Three-phase to ground faults (L-L-L-G) and three-phase faults (L-L-L) are the two varieties of symmetrical faults. The simulation results for a (L-L-L-G) scenario with SFCL are shown in Figure 10. Symmetrical faults occur when faults happen in all three phases of the system. The three-phase fault is depicted in Fig.10, and upon analyzing the results, it is evident that the current reaches a value of  $1.1 \times 10^4$  amperes. To limit this current, the SFCL is introduced to reduce it to a level that can be safely interrupted by opening the mechanical switch. Simultaneously, a reverse voltage of 1400 volts is applied. This process took place from the moment the fault started until it was cleared at time 0.11 seconds.

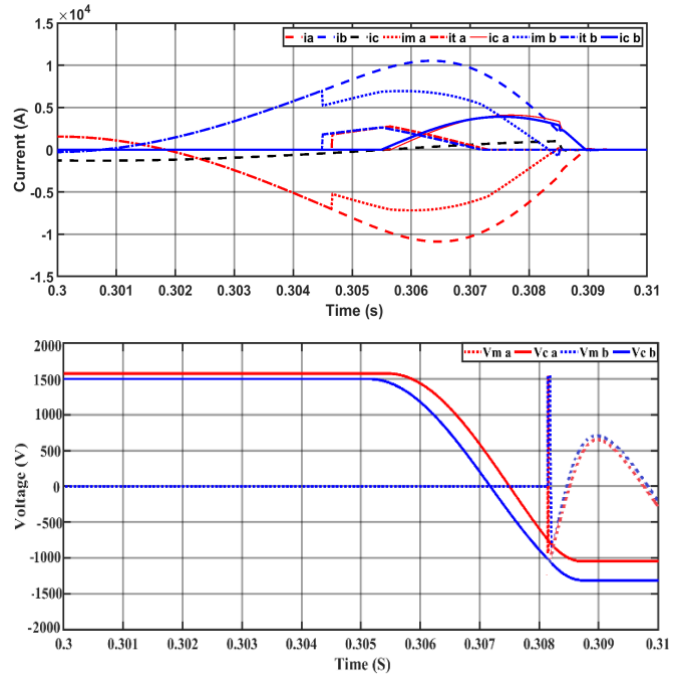


**Fig.9.** Current and voltage waveforms using SFCL at L-L fault at phase A & B

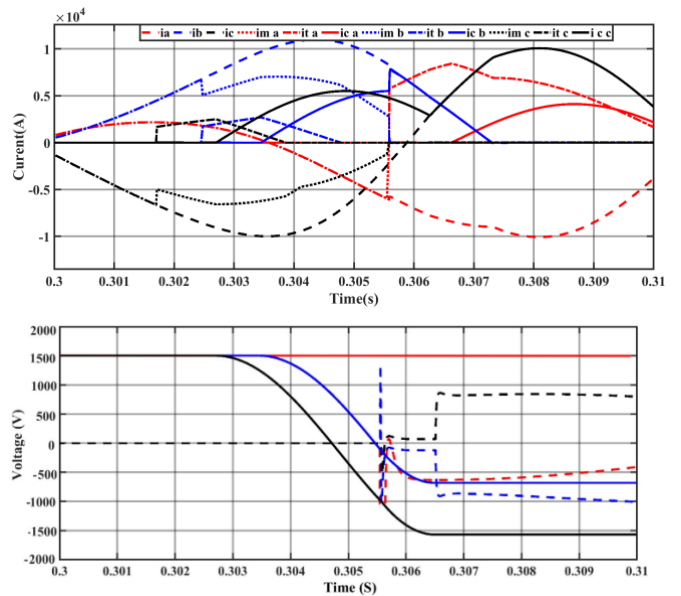


**Fig. 10.** Three-phase fault current and voltage waveforms using SFCL

Because current values in all phases surpasses the  $I_{max}$  value or the predefined discrimination current value, the findings shown in Table 1 show that all SFCL units function properly. In this instance, the entire system is interrupted. These findings suggest that SFCL can effectively handle any kind of three-phase failure in a three-phase system. Since the current in all phases exceeds the  $I_{max}$  or the predetermined discrimination current value, the data in Table 1 demonstrate that all SFCL units are in good working order. Due to SFCL's effective operation, the system in this particular instance completely breaks down. These results indicate that different symmetrical fault types in a three-phase system can be efficiently addressed by SFCL.



Table 1: Comparison between different faults with SFCL

Type of faults	S.L. G			L.L. G			3L. G
	A-G	B-G	C-G	AB-G	AC-G	BC-G	ABC-G
$I_{max}$	4000	6000	3400	$1.1 \cdot 10^4$	$0.7 \cdot 10^4$	$1.1 \cdot 10^4$	$1.1 \cdot 10^4$
$V_{rec}$	1300	1500	1200	1500	1500	1400	1400
$T_{int}$	0.01	0.01	0.07	0.09	0.05	0.06	0.11

4.2 Effects of the Making Angle on the SFCL Operation

One of the significant factors that greatly affect the behavior of an AC hybrid C.B is the angle of fault making. The making angle refers to the phase angle at which the S.C event begins. It is measured from the point when the source voltage reaches zero, following the occurrence of the positive voltage sine half-wave, to the moment when the short-circuit event initiates.

Conversely, several crucial parameters are associated with the C.B. The commutation time, the amount of time until the recovery voltage appears, the peak recovery voltage across the mechanical switch, and the highest charging voltage of the commutation capacitor are some of these factors. These parameters are dependent on factors such as the rate of change of current (di/dt) and the maximum fault current magnitude.

The making angle is widely recognized for its significant impact on both the value of current rise (di/dt) and the maximum fault current magnitude. Specifically, when the circuit is closed precisely at the voltage zero cross-over point, the short-circuit current reaches its maximum value, denoted as  $I_{Max}$ , while the lowest initial rate of current rise (di/dt) is observed at this angle. Conversely, the highest initial rate of current rise (di/dt) occurs when the fault is initiated at a 90-degree making angle.

The initial rate of current rise (di/dt) during a fault occurrence is a more crucial metric from the standpoint of SFCL functioning than the maximum fault current amplitude. The di/dt and the maximum fault current are greatly impacted by the fault-making angle, lengthening the commutation period. When the circuit is closed at the voltage zero cross-over point (fault making angle  $\psi = 0$ ), the time it takes for the recovery voltage to appear, written as  $\Delta t_2$ , reaches its maximum value. Additionally, the commutation time, shown by the symbol  $\Delta t_1$ , achieves its minimal value at this angle. In contrast, a 90-degree fault-making angle is formed by the minimum value of  $\Delta t_2$  and the greatest value of  $\Delta t_1$ .

4.2.1 Fault at 0 Degree Making

Figure 11 depicts the simulation results of current and voltage behavior when utilizing the Hybrid circuit breaker with SFCL in the case of SLG fault occurring at a 0-degree angle. The simulation showcases how the SFCL system behaves in response to a specific fault condition. It's important to understand how the current and voltage respond to this fault. In this case, the fault occurs at a 0-degree angle with respect to the voltage waveform. This angle affects the timing and amplitude of the fault current. Figure 11 illustrates the current on Phase A during a one-sided fault application between Phase A and ground at an angle of zero degrees. It is observing an increase in current to 5800 amperes at time 0.32 seconds, which exceeds the set current value for SFCL. In this scenario, the current is limited to a level where a reverse

voltage of 1500 volts is applied across the mechanical switch terminals. This process took place from the moment the fault started until it was cleared at time 0.014 seconds.

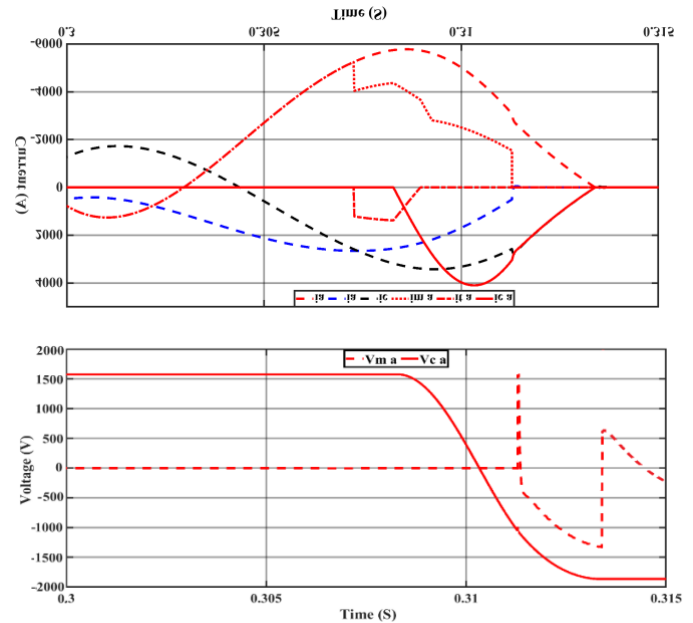


Fig.11. Current and voltage waveforms SFCL at SLG fault at 0 angles.

4.2.2 Fault at 90 Degree Making

Figure 12 illustrates the simulation results of the current and voltage behavior when implementing the high-speed circuit breaker with SLG fault at a fault making angle of 90 degrees. It visually represents how the system responds to this specific scenario. Figure 12 demonstrates a one-sided fault application between Phase A and ground at an angle of 90 degrees. It is observing an increase in the current to 5600 amperes at time 0.305 seconds, at which point SFCL is immediately activated. In this case, the current is limited to a level where a reverse voltage of 1100 volts is applied across the mechanical switch terminals. This process took place from the moment the fault started until it was cleared at time 0.09 seconds.

4.2.3 Fault at 170 Degree Making

Figure 13 provides a unique illustration of how the SFCL functions when dealing with a SLG fault that occurs precisely at the midpoint of the AC waveform cycle (170 degrees angle). The SFCL ability to respond quickly and effectively to faults is instrumental in maintaining the electricity network's security and stability. Figure 13 depicts a fault occurring at an angle of 170 degrees. At this point, the current reaches a value of 5900 amperes at time 0.31, and SFCL is promptly engaged. SFCL significantly and rapidly limits the current to a level where the mechanical switch can be opened without generating any electrical arcing. This is achieved by applying a reverse voltage of 2350 volts across the switch terminals. The entire process, from the fault initiation to clearing, took place over a period of 0.013 seconds.

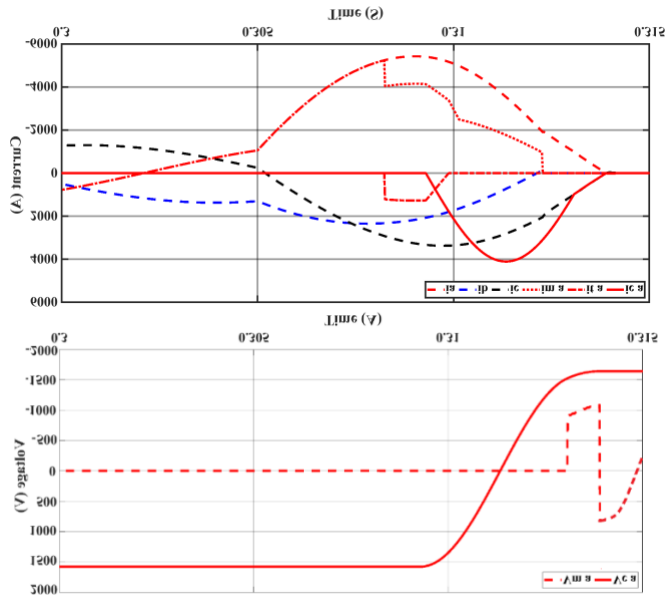


**Fig.12.** Current and voltage simulation SFCL with SLG fault at 90 faults making angle

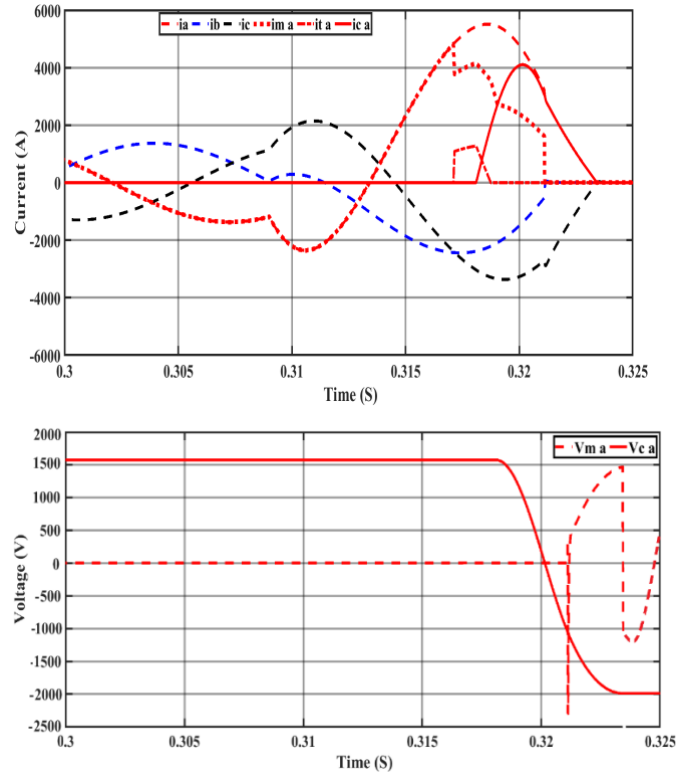
The fault making angle signifies the instant within the AC waveform cycle when the fault initiates. In this specific case, the fault is presented near at the midpoint of the waveform cycle, which is 170 degrees. At this point, the AC voltage waveform is crossing the zero-voltage axis, transitioning from the positive half-cycle. The protective devices, containing the SFCL, are triggered by the abrupt disturbance in current due to the fault. Their purpose is to confirm the safety and integrity of the electrical system by rapidly responding to abnormal conditions.

Table 2 summarizes the performance of the SFCL in response to faults occurring at different angles within the system. The comparison primarily focuses on the SLG fault type, and how effectively the SFCL, referred to as **SFCL**, manages these faults.

**4.3 Effect of Faults Location**

**4.3.1 The Fault Occurs Close to the Load (FLC1)**

In this section, we examine the influence of fault location near the load while incorporating the SFCL. This scenario, denoted as FLC1, explores how the presence of SFCL affects the power system's response to faults occurring in proximity to the load. The objective is to understand how SFCL intervention impacts fault current mitigation and overall system stability in this specific location. The presented Fig. 14, show cases the outcomes of a comprehensive current and voltage simulation, incorporating the SFCL within a scenario where a fault occurs in proximity to the load, termed as FLC1. The location of the fault is one of the most critical factors to analyze. Therefore, Fig. 14 illustrates a fault occurring near the load. In this case, we observe the current reaching 1600 amperes at time 0.308, and SFCL is immediately activated. SFCL limits the current to a level where the mechanical switch can be safely opened without causing any electrical arcing. This is achieved by applying a reverse voltage of 500 volts across the switch terminals. The entire process, from the initiation of the fault to clearing, takes place over a period of 0.012 seconds.



**Fig.13.** Current and voltage simulation SFCL with SLG fault at 170 faults making angle

Table 2: Comparison between different angle faults with SFCL

Angle	0	30	90	120	150	170	270
$I_{max}$	5800	5800	5600	5800	5700	5900	5600
$V_{rec}$	1500	1300	1100	1300	1400	2350	1100
$T_{fault}$	0.32	0.301	0.305	0.306	0.308	0.31	0.315
$T_{int}$	0.014	0.012	0.09	0.08	0.015	0.013	0.09

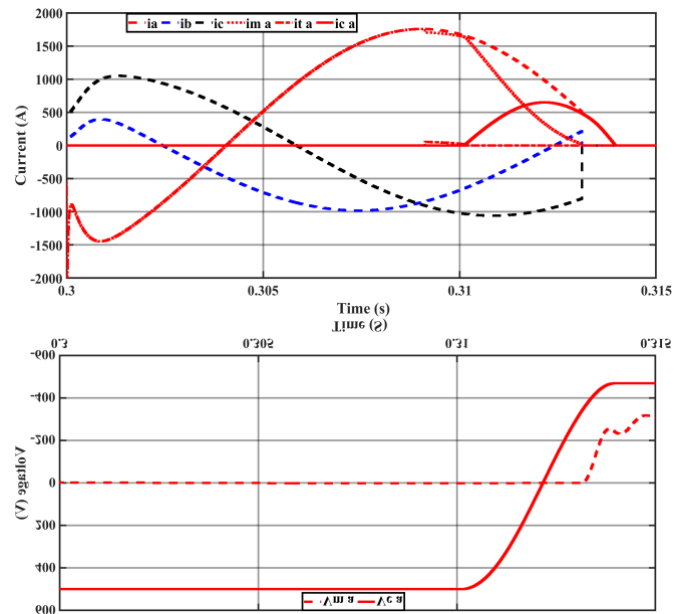


**Fig. 14.** Current and voltage simulation SFCL at the fault occurs close to the load (FLC1)

**4.3.2 The Fault Occurs Close to the Grid (FLC<sub>2</sub>)**

Moving forward, in this paper, investigate the impact of faults near the grid while utilizing SFCL, referred to as FLC<sub>2</sub>. By incorporating SFCL technology, the aim to assess how faults occurring in the vicinity of the grid are handled. This analysis provides insights into how the grid-connected components, coupled with SFCL, respond to faults, leading to enhanced fault clearance and improved the grid reliability. Figure 15 presents an insightful visual representation of current and voltage dynamics during a fault close to the grid, incorporating the use of SFCL. The analysis of a fault occurring in another location near the power grid is presented in Fig. 15. In this case, we observe the current reaching 4100 amperes at time 0.311 seconds, and SFCL is applied to manage the fault by limiting it to the desired value. This is achieved by applying a reverse voltage of 1600 volts across the SFCL terminals. The entire process, from the initiation of the fault to clearing, took place over a period of 0.013 seconds.

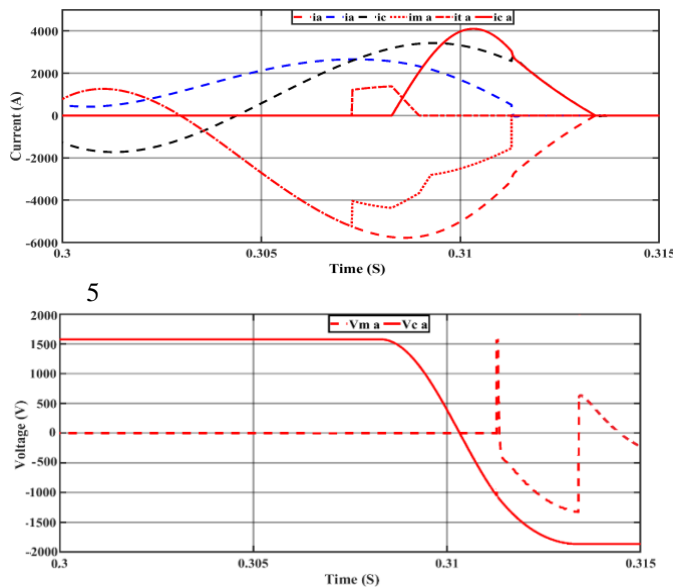


**Fig.15.** Current and voltage simulation SFCL at the fault occurs close to the Grid (FLC<sub>2</sub>)

**4.3.3 The Fault Occurs Close to the Wind & PV (FLC<sub>3</sub>)**

Within this subsection, delve into the effects of faults occurring near wind and PV systems, while also implementing SFCL. Referred to as FLC<sub>3</sub>, this investigation explores how SFCL intervention influences fault behavior in the vicinity of renewable energy sources. Understanding how SFCL interacts with faults in this context sheds light on its potential to safeguard renewable energy systems. Figure 16, provides a visual narrative of current and voltage behaviors during a fault occurrence near wind and PV systems, with the implementation of SFCL. By focusing on this context, stakeholders gain valuable insights into SFCL pivotal role in enhancing the reliability, stability, and resilience of renewable energy systems. Lastly, a fault near the Wind & PV system is presented in Fig. 16. SFCL is introduced to limit the current, which had a maximum value of 1000 amperes. Subsequently, a reverse voltage of 800 volts is applied to the switch, and no electrical arcing is observed. This entire process occurred at time 0.08 seconds.

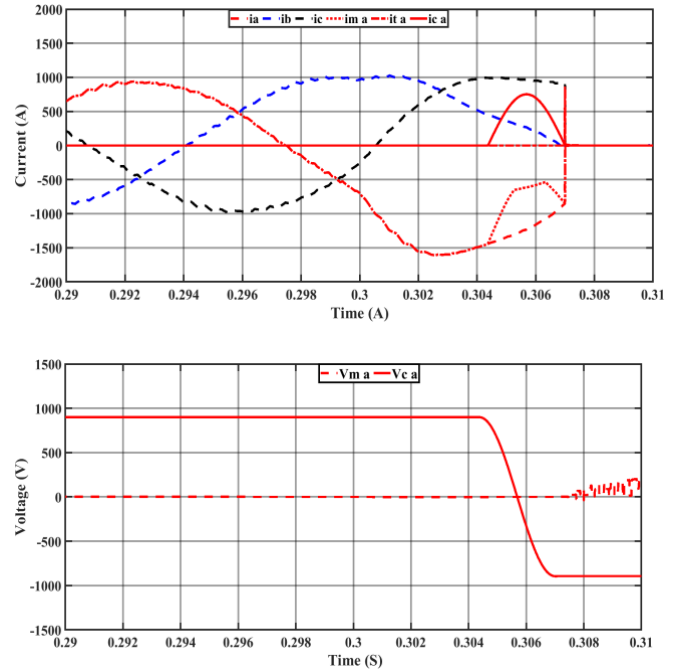


**Fig.16.** Current and voltage simulation SFCL at the fault occurs close to the Wind & PV (FLC<sub>3</sub>)

The choice of fault location has a direct impact on how SFCLs perform. Their ability to reduce fault currents and enhance system stability is particularly useful near loads and in grid-connected scenarios. Moreover, SFCLs play a crucial role in protecting renewable energy sources from fault-induced disturbances. This emphasizes the versatility and effectiveness of SFCLs in different failure scenarios, underscoring their importance in the reliability and resilience of modern power systems.

**5. Conclusions**

This comprehensive study has showcased the robustness and versatility of SFCLs within the context of a Microgrid environment. SFCLs play a pivotal role in mitigating the impact of grid disturbances in transmission and distribution systems, with an impressive reduction in fault current of up to 80% in diverse fault scenarios. To lessen the impact of grid disturbances, transmission and distribution systems use SFCLs. It highlighted SFCL's effectiveness across diverse fault types and locations, as well as its sensitivity to operational parameters like the making angle. The findings underscore SFCL's potential to enhance fault management, stability, and reliability in modern power systems. The collective insights provide valuable guidance for power system engineers, aiding in the optimal deployment of SFCLs to enhance power network performance and resilience. This research contributes to the advancement of power system protection strategies, ensuring a more secure and efficient energy infrastructure. The research explored the impact of different fault types on the effectiveness of SFCL. The study has illuminated the effectiveness of SFCLs across various fault types and locations while highlighting their sensitivity to operational parameters, especially the making angle. It is notable that the making angle can significantly impact the inrush current, with a reduction of up to 70% observed with optimal SFCL operation. This underscores SFCL's

adaptability and suitability for diverse fault scenarios. It was found that the making angle significantly affects the inrush current and the subsequent behavior of SFCL. This insight is crucial for optimizing SFCL operation and ensuring its reliability during fault events. It covered fault occurrences near loads, the grid, and renewable energy sources within a Microgrid setup. The results indicated SFCL's consistent ability to limit fault currents in many fault sites, ensuring the stability and dependability of the system.

**Funding:** This work is funded and supported by the Deanship of Scientific Research, Taif University

**Acknowledgments:** The researchers would like to acknowledge the Deanship of Scientific Research, Taif University for funding this work

## References

- [1] F. Zheng, C. Deng, L. Chen, S. Li, Y. Liu and Y. Liao, "Transient Performance Improvement of Microgrid by a Resistive Superconducting Fault Current Limiter," in *IEEE Transactions on Applied Superconductivity*, vol. 25, no. 3, pp. 1-5, June 2015.
- [2] U. A. Khan, J. K. Seong, S. H. Lee, S. H. Lim and B. W. Lee, "Feasibility Analysis of the Positioning of Superconducting fault current limiters for the Smart Grid Application Using Simulink and Sim Power System," in *IEEE Transactions on Applied Superconductivity*, vol. 21, no. 3, pp. 2165-2169, June 2011.
- [3] A.M. Hamada, S. A. M. Abdelwahab, S. Hasan, R. Salem, W. S. E. Abdellatif, "Design and Experimental Investigation of Three-Phase Inductive Type Superconducting Fault Current Limiter based on Current Injection Method," *International Journal of Renewable Energy Research-IJRER*, vol 13, no 3, 2023.
- [4] L. Chen; Hongkun Chen; Jun Yang; Lin Zhu; Yi Tang; Leong Hai Koh; Ying Xu; Chi Zhang; Yuxiang Liao; Li Ren "Comparison of Superconducting Fault Current Limiter and Dynamic Voltage Restorer for LVRT Improvement of High Penetration Microgrid," in *IEEE Transactions on Applied Superconductivity*, vol. 27, no. 4, pp. 1-7, June 2017.
- [5] H. He; L. Chen; T. Yin; Z. Cao; J. Yang; X. Tu; L. Ren, "Application of a SFCL for Fault Ride-Through Capability Enhancement of DG in a Microgrid System and Relay Protection Coordination," in *IEEE Transactions on Applied Superconductivity*, vol. 26, no. 7, pp. 1-8, Oct. 2016.
- [6] S. Sugimoto, J. Kida, H. Arita, C. Fakui, and T. Yamagiwa, "Principle and characteristics of a fault current limiter with series compensation," *IEEE Trans. Power Delivery*, vol. 11, no. 2, pp. 842-847, 1996.
- [7] T. Jamasb, W. J. Nuttall, and M. G. Pollitt, *Future Electricity Technologies and Systems*. Cambridge: Cambridge Univ. Press, pp. 83- 97, 235-246, 2006.
- [8] B. C. Sung, D. K. Park, J. W. Park, and T. K. Ko, "Study on a series resistive SFCL to improve power system transient stability: Modeling, simulation and experimental verification," *IEEE Trans. Industrial Electron.*, vol. 56, no. 7, pp. 2412-2419, 2009.
- [9] M. Naresh, N. K. Singh and A. K. Singh, "Superconducting fault current limiter for grid connected power system protection," 2016 IEEE International Conference on Industrial Technology (ICIT), Taipei, Taiwan, 2016, pp. 576-581.
- [10] E. Dehghanpour, H. Kazemi Karegar, R. Kheirollahi and T. Soleymani, "Optimal Coordination of Directional Overcurrent Relays in Microgrids by Using Cuckoo-Linear Optimization Algorithm and Fault Current Limiter," in *IEEE Transactions on Smart Grid*, vol. 9, no. 2, pp. 1365-1375, March 2018.
- [11] Jo, H.C.; Joo, S.K.; Lee, K. Optimal placement of superconducting fault current limiters (SFCLs) for protection of an electric power system with distributed generations (DGs). *IEEE Trans. Appl. Supercond.* 2013, 23, 3-6.
- [12] Ye, L.Y.L.; Lin, L.L.L.; Juengst, K.-P. Application studies of superconducting fault current limiters in electric power systems. *IEEE Trans. Appl. Supercond.* 2002, 12, 900-903.
- [13] Hatta, H.; Muroya, S.; Nitta, T.; Shirai, Y.; Taguchi, M. Experimental study on limiting operation of Superconducting Fault Current Limiter in double circuit transmission line model system. *IEEE Trans. Appl. Supercond.* 2002, 12, 812-815.
- [14] Li, B.; Li, C.; Guo, F.; Xin, Y.; Wang, C.; Pang, X. Coordination of superconductive fault current limiters with zero-sequence current protection of transmission lines. *IEEE Trans. Appl. Supercond.* 2014, 24.
- [15] Llambes, J.C.H.; Hazelton, D.W.; Weber, C.S. Recovery under load performance of 2nd generation HTS superconducting fault current limiter for electric power transmission lines. *IEEE Trans. Appl. Supercond.* 2009, 19, 1968-1971.
- [16] Abdellatif, W.S.E., Hamada, A.M. & Abdelwahab, S.A.M. "Wind speed estimation MPPT technique of DFIG-based wind turbines theoretical and experimental investigation. *Electr Eng* 103, 2769-2781 (2021). <https://doi.org/10.1007/s00202-021-01268-8>
- [17] M. A. E. Eid, S. A. M. Abdelwahab, H. A. Ibrahim and A. H. K. Alaboudy, "Improving the Resiliency of a PV Standalone System Under Variable Solar Radiation and Load Profile," 2018 Twentieth International Middle East Power Systems Conference (MEPCON), Cairo, Egypt, 2018, pp. 570-576, doi: 10.1109/MEPCON.2018.8635160.
- [18] A. Elnozohy, A. M. Yousef, F. K. Abo-Elyousr1, M. Mohamed and S. A M. Abdelwahab "Performance improvement of hybrid renewable energy sources connected to the grid using artificial neural network and sliding mode control', *J. Power Electron.* 21, 1166-1179 (2021). <https://doi.org/10.1007/s43236-021-00242-8>
- [19] A. H. K. Alaboudy, A. M. Azmy, and W.S.E. Abdellatif, "Controller performance of variable speed wind driven doubly-fed induction generator," *IEEE Saudi Arabia Smart Grid (SASG)*, 7-9 Dec. 2015.
- [20] Saleh, B., F. K. Abo-Elyousr, A. Elnozahy, M. Mohamed S. A. M. Abdelwahab, " Design of PID Controller with Grid Connected Hybrid Renewable Energy System Using Optimization Algorithms", *J. Electr. Eng.*

- Technol. 16, 3219–3233 (2021).  
<https://doi.org/10.1007/s42835-021-00804-7>.
- [22] S. A. M. Abdelwahab, A. A. Elbaset, F. Yousef, W. S.E. Abdellatif, "Performance Enhancement of PV Grid Connected Systems with Different Fault Conditions," International Journal on Electrical Engineering & Informatics, Vol. 13 No. 4, December 2021.
- [23] A.M. Hamada, S. S.M. Ghoneim, S. A. Mohamed Abdelwahab, W. S.E. Abdellatif, "Performance analysis of three-phase hybrid fault current limiter with one commutation circuit," International Journal of Electrical Power & Energy Systems, Vol. 133, 2022.
- [24] D. Mansour, D. Yehia, "Analysis of 3-phase superconducting fault current limiters in power systems with inhomogeneous quenching", IEEE Transactions on Applied Superconductivity, Vol.23, pp.5602605-5602605, 2013.
- [25] S. M. Blair, M., C. D. Booth and G. M. Burt; "Current–Time Characteristics of Resistive superconducting Fault Current Limiters", IEEE Transactions on Applied Superconductivity, Vol. 22, NO. 2, 2012.
- [26] H. Bakiri, H. Maziku, N. Mvungi, N. Hamisi, Massawe Libe, " A Novel Load Forecasting Model for Automatic Fault Clearance in Secondary Distribution Electric Power Grid using an Extended-Multivariate Nonlinear Regression", International Journal of Smart Grid, Vol.5, no.2, June, 2021.
- [27] R. Faisal, Badal, K. S. Sarker, S. K. Das, " Transient Stabilization Improvement of Induction Generator Based Power System using Robust Integral Linear Quadratic Gaussian Approach", International Journal of Smart Grid, Vol.3, no.2, June, 2019.
- [28] D. Varela, R. Oliveira, L. Romba and J. Murta-Pina, "A Superconducting Saturable Core Reactor for Power Flow Control in Transmission Grids," 2021 9th International Conference on Smart Grid (icSmartGrid), Setubal, Portugal, 2021, pp. 216-219.
- [29] F. Banihashemi, S. Beheshtaein and R. Cuzner, "Novel Hybrid Circuit Breaker Topology Using a Twin Contact Mechanical Switch," 2021 9th International Conference on Smart Grid (icSmartGrid), Setubal, Portugal, 2021, pp. 132-136.
- [30] K. Naraghipour, K. Ahmed and C. Booth, "New Islanding Detection Method With Voltage Amplitude Variation for Inverter-based Distributed Generator," 2021 9th International Conference on Smart Grid (icSmartGrid), Setubal, Portugal, 2021, pp. 243-248.
- [31] Chang, C.S. and Loh, P.C.; "Integration of Fault Current Limiters on Power System for Voltage Quality Improvement", Electric power systems research, Vol 57, 2001.